Journal Name

ARTICLE

High-performance Oxygen Reduction Reaction Fuel Cell Catalysts Containing Only Atomically Dispersed Iron Active Sites

Received 00th January 20xx,
Accepted 00th January 20xx

DOI: 10.1039/x0xx00000x

www.rsc.org/

Hanguang Zhang,[a] Hoon T. Chung,[b] David A. Cullen,[c] Stephan Wagner,[d] Ulrike I. Kramm,[d] Karren L. More,[e] Piotr Zelenay,[b,*] and Gang Wu[a,*]

Abstract: Platinum group metale-free (PGM-free) catalysts for the oxygen reduction reaction (ORR) with atomically dispersed FeN_4 sites have emerged as a potential replacement for low-PGM catalysts in acidic polymer electrolyte fuel cells (PEFCs). In this work, we carefully tuned doped Fe content into zeolitic imidazolate framework (ZIF)-8 precursors and achieved complete atomic dispersion of FeN_4 sites, the sole Fe species in the catalyst based on Mößbauer spectroscopy data. The Fe-N-C catalyst with the highest density of active sites achieved respectable ORR activity in rotating disk electrode (RDE) testing with a half-wave potential ($E_{½}$) of 0.88 ± 0.01 V *vs*. the reversible hydrogen electrode (RHE) in 0.5 M H_2SO_4 electrolyte. Activity degradation was found to be more significant when holding a potential at 0.85 V relative to the standard potential cycling (0.6-1.0 V). The post-mortem analysis provides insights into possible catalyst degradation mechanisms associated with Fe-N coordination cleveage and carbon corrosion. High ORR activity was confirmed in fuel cell testing, which also divulged promising performance of the catalysts at practical PEFC voltages. We conclude that the key factor behind the high ORR activity of the Fe-N-C catalyst is an optimum Fe content in the ZIF-8 precursor. While too little Fe in precursors results in insufficient density of FeN_4 sites, too much of Fe leads to the formation of clusters and ensuing significant loss in catalytic activity due to the loss of atomically dipsered Fe to the inactive clusters or even nanoparticles. Advanced electron microscopy was used to obtain insights into the clustering of Fe atoms as a function of the doped Fe content. The Fe content in the precursor also affects other key catalyst properties such as the particle size, porosity, nitrogen-doping level, and carbon microstructure. Thanks to using the model catalysts exclusively containing FeN_4 sites, it was possible to directly correlate ORR activity with the density of FeN_4 species in the catalyst.

Introduction

The high cost and less than desirable performance of platinum group metal (PGM) catalysts for oxygen reduction reaction (ORR) represent two big challenges facing the acidic polymer electrolyte fuel cell (PEFC) technology. In this context, PGM-free catalysts emerge as an appealing alternative, provided they can fulfill the stringent activity and durability requirements of practical systems. Among various PGM-free catalysts developed to date, the iron and nitrogen co-doped carbon catalysts (Fe-N-C) have shown encouraging activity and stability.[1-3] Spectroscopic studies and computational simulations suggest that FeN_4, and possibly other similar Fe-N species, are the likely active sites for the ORR in such catalysts.[4-6] Increasing the density of FeN_4 sites by atomically dispersing Fe in catalyst precursors appears to be an effective strategy for enhancing catalytic activity.[6-8] Relative to other precursors, Zn-rich zeolitic imidazolate frameworks (ZIF-8), with potentially capability to host FeN_4 moieties as their key structural element are especially attractive for achieving high density of FeN_4 sites in catalysts obtained using one-step high-temperature thermal activation approach.[3, 8-17] The synthesis of ZIF-8-derived catalysts typically does not require carbon-black supports and tedious post treatments such as acidic leaching and multiple heat treatments).[17-20] Nevertheless, the ORR activity of many ZIF-8-derived catalysts is often low in acidic media, likely due to insufficient density of FeN_4 sites resulting from the loss of Fe to the ORR-inactive metal-rich aggregates[21-23] and poor control over the Fe dispersion in catalysts. While the metal content in catalysts has been recognized as one of the critical factors affecting ORR performance of Fe-N-C catalysts,[17, 24-27] little is known about the role of Fe during the active site formation and chemical forms of Fe involved in the ORR. The lack of well-defined Fe-N-C catalysts, with homogeneous morphology and uniform active-site dispersion has made rational design and fundamental knowledge gaining in this area even more challenging.

[a] *Department of Chemical and Biological Engineering, University at Buffalo, The State University of New York, Buffalo, New York 14260, United States. E-mail: gangwu@buffalo.edu*
[b] *Materials Physics & Applications Division, Los Alamos National Laboratory, Los Alamos, New Mexico 87545, United States. E-mail: zelenay@lanl.gov*
[c] *Materials Science and Technology Division, Oak Ridge National Laboratory, Oak Ridge, Tennessee 37831, United States*
[d] *Technische Universität Darmstadt, Department of Materials- and Earth Sciences and Department of Chemistry, 64287 Darmstadt, Germany*
[e] *Center for Nanophase Materials Sciences, Oak Ridge National Laboratory, Oak Ridge, Tennessee 37831, United States*
† Footnotes relating to the title and/or authors should appear here.
Electronic Supplementary Information (ESI) available: [details of any supplementary information available should be included here]. See DOI: 10.1039/x0xx00000x

In this work, we employed chemical doping to replace a small fraction of Zn ions in ZIF-8 precursors with Fe ions.[17] This approach allowed for precise control of the Fe content in the imidazolate precursors to study its effect on catalytic properties and ORR activity. The ZIFs have been identified as ideal precursors capable of providing imidazolate ligands to coordinate Fe sites in FeN_4 complexes within a 3D ZIF framework. Thus, chemical doping of Fe into ZIF-8s allows for better Fe dispersion in the precursor and precise control over the Fe content. Through subsequent high-temperature treatment, chemically Fe doped ZIFs are directly converted into high surface-area carbons, co-doped with Fe and N.[17, 21, 28, 29] Zn evaporation during the heat treatment benefits the formation of porous carbon phases making active sites accessible during the ORR.[22, 30, 31]. By carefully tuning the doped Fe content, we synthesized model Fe-N-C catalysts with atomically dispersed and nitrogen coordinated FeN_4 sites uniformly dispersed in partially graphitized carbon phases, and without any formation of Fe-rich aggregates. Mößbauer spectroscopy verified the exclusive presence of Fe in the FeN_4 form. The advanced electron microscopy helped to monitor the Fe clustering process with an increase of Fe doping content in ZIF-8 precursors. The effect of Fe content on physical and catalytic properties was systematically studied. Catalysts with the highest FeN_4 density achieved a record ORR activity in acidic electrolytes, significantly minimizing the gap to the start of the art Pt/C catalysts. The atomically dispersed Fe catalysts were further studied in fuel cells, which showed promising performance and improvements to durability at practical operation voltages.

Results and Discussion

Atomic Fe site dispersion in catalysts

The Fe content in Fe-doped ZIF-8 (Fe-ZIF) was controlled by replacing part of the original Zn ions with Fe ions during the solution-phase synthesis of nanocrystalline ZIF-8 precursors in methanol.[32] The catalysts were labelled *x*Fe-ZIF, where *x* represents the atomic content of Fe^{3+} relative to the total content of metal ions (Fe^{3+} and Zn^{2+}) in ZIF-8 precursors in the range from 0.1 to 9.0 at.%. A single-step heat treatment at 1100 °C under an inert atmosphere flow was optimized to convert Fe-doped ZIF precursors directly into *x*Fe-ZIF catalysts without any additional post-treatments. Detailed synthesis procedures and extensive characterization methods are described in Electronic Supplementary Information (ESI). Figure S1 in ESI shows the synthesis scheme.

High angle annular dark field scanning transmission electron microscope (HAADF-STEM) images in **Figures 1a-b** attest to the atomic and uniform dispersion of Fe atoms in the carbon phase. The two images shown, recorded for the same area in the best performing 1.5Fe-ZIF catalyst in the bright field and Z-contrast modes, respectively, are representative of the entire catalyst sample. The electron energy loss spectroscopy (EELS) revealed the tendency for the iron and nitrogen atoms to be co-located in the catalyst, directly suggesting coordination of Fe by N (**Figures 1c-d**). With an increase in the doped Fe content in ZIF-8 precursors, the transition from atomically dispersed Fe sites to Fe clusters was observed (**Figures 1e-1h**). Clustering appeared in the catalyst derived from the precursor with 2.5 at% of Fe and became prevalent in the catalyst generated from the precursor with 3.0 at% of Fe (see EELS data in the inset in **Figure 1h**). These ultra-high resolution STEM data confirm the key role of atomically dispersed Fe sites in the ORR. It also explains the best activity of the 1.5Fe-ZIF catalyst due to the highest density of atomic Fe sites without any Fe clustering. A decrease in the ORR activity with further increase in the Fe content is due to a gradual loss of atomically dispersed Fe to clusters and, ultimately, to Fe-rich nanoparticles.

Unlike in the earlier reported Fe-N-C catalysts having highly heterogeneous morphology,[33] the atomically dispersed catalyst with an optimum Fe content benefits from the conversion of all available Fe in the precursor to the FeN_4 active sites, rather than to the less active clusters or nanoparticles. The possible reason for the high Fe utilization in the catalyst is ligation of Fe atoms in precursors by 2-methylimidazole and their spatial separation by Zn atoms within the ZIF-8 structure. The ligation of Fe atoms reduces their mobility and assures uniform distribution throughout the precursor, also during the follow-up high-temperature treatment.[34] The spatial isolation prevents the formation of Fe-rich (Fe and/or Fe_3C) aggregates during the heat treatment. The coordination bonds between Zn^{2+} ions and 2-methylimidazole in precursors are broken at around 500 °C, with zinc ions undergoing likely reduction to metallic Zn.[12] This leads to the reduction in microporosity and surface area. Subsequent removal of metallic zinc species above 800 °C *via* evaporation gradually recovers catalyst surface areas, though not to the original level (**Figure S2**). When Fe content in the precursor exceeds *ca.* 1.5 at.%, a fraction of Fe atoms, which can no longer be accommodated by the ZIF matrix, undergo agglomeration and ultimately conversion to Fe- and/or Fe_3C-rich clusters and nanoparticles during the high-temperature treatment. These forms of Fe do not contribute to the ORR activity in the acidic solution (at all or to a negligible level); to the contrary, their formation may cause a decrease in the content of atomically dispersed Fe sites in the catalyst, probably due to larger strength of Fe-Fe bonds than Fe-N bonds.[35]

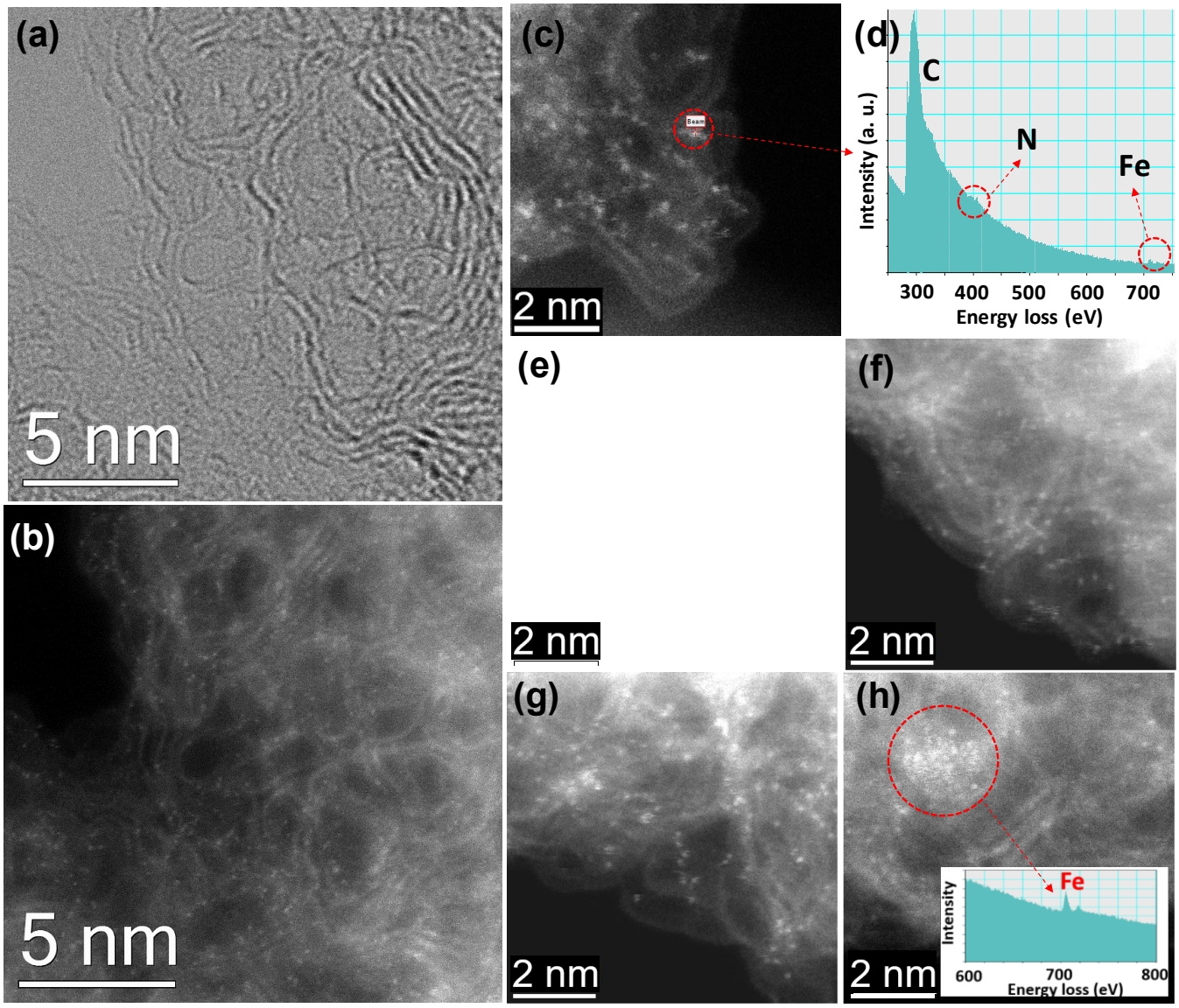

Figure 1. Atomic dispersion of Fe sites in Fe-doped ZIF catalysts. (**a**) Bright-field STEM image showing partially graphitized carbon fringes in the best performing 1.5Fe-ZIF catalyst; (**b**) HAADF-STEM image of the same depicting the single Fe sites (bright dots) dispersed throughout the carbon phase in the 1.5Fe-ZIF catalyst; (**c-d**) Fe-N-C structure analyzed by HAADF-STEM and EELS, respectively; (**e-h**) evolution of atomically dispersed Fe sites to Fe-rich aggregates with an increase in iron content in ZIF precursors with 0.05Fe-ZIF (**e**), 1.5Fe-ZIF (**f**), 2.5Fe-ZIF (**g**) and 3.0Fe-ZIF (**h**). (Fe clusters beginning to form in catalyst derived from Fe-ZIF precursor 2.5 at.% of Fe); EELS confirmation of cluster formation shown in the inset in (**h**).

Our previous DFT and experimental X-ray absorption spectroscopy (XAS) studies suggest that FeN_4 is likely the active site in Fe-N-C catalysts.[16, 36] Highly iron-sensitive Mößbauer spectroscopy experiments were further carried out with the most active 1.5Fe-ZIF catalyst for more than 20 days to assure sufficient Fe signal. The result shown in **Figure 2a** indicates that Mößbauer parameters of the doublets D1 and D2 are associated with Fe species in FeN_4 configuration (**Figure 2c**). D1 is interpreted in terms of an in-plane FeN_4 coordination integrated in graphene layers. D2 is accounted for by a FeN_{2+2} coordination with a pseudo-sixfold coordination of Fe by the four neighboring nitrogen atoms and carbon or nitrogen atoms in the axial direction from graphene planes above and below (cf. the crystal structure of FePc).[37-39] Our previous DFT calculations suggest that the FeN_4C_8 moiety should have higher intrinsic activity than the FeN_4C_{10} moiety.[36] Based on these results and previouscorrelation of activity vs. Mößbauer species,[40] D1 may act similar to FeN_4C_8. It was predicted that the carbon atoms with dangling bonds adjacent to FeN_4 moieties are part of the ORR active sites, which bind the OOH intermediate to facilitate the cleavage of O-O bonds during the ORR. The Fe valence is close to 2+ in the catalysts, which is in good agreement with our previous XAS analysis suggesting a valence between 3+ and 2+.[16] It should be noted that the Fe catalysts were exposed to air before the analysis, causing possible oxidation. The valance can be changed depending on applied potentials during the ORR. The uncertainty in the accurate determination of the Fe valence at the catalyst surface notwithstanding, Mößbauer

results confirm the exclusive atomic dispersion of FeN_4 sites in the catalyst and the absence of any other Fe crystalline phases, such as metal, oxide, carbide, or nitride.

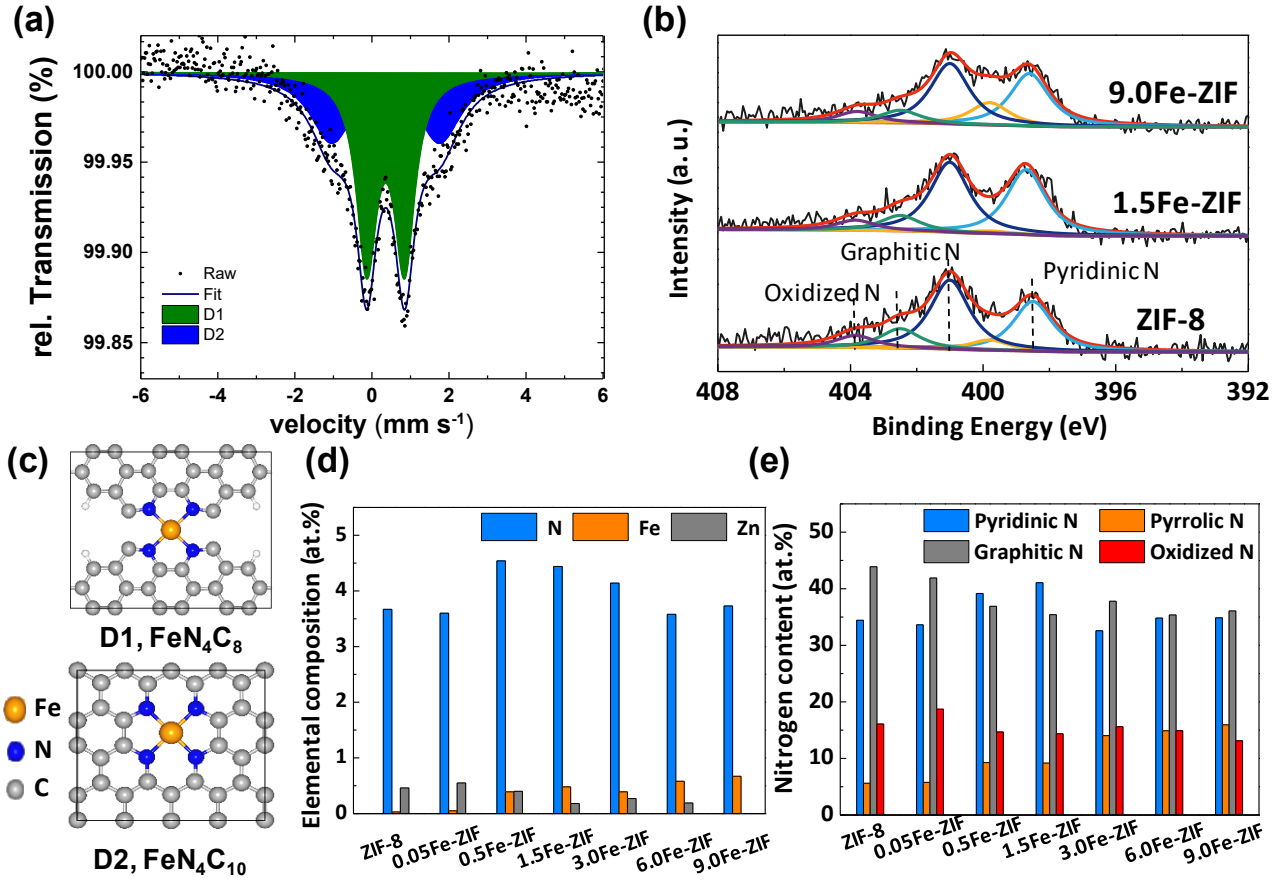

Figure 2. (**a**) Mößbauer spectroscopy of the best performing atomically dispersed Fe catalyst (1.5Fe-ZIF); (**b**) XPS N1s spectra of ZIF-8, 1.5Fe-ZIF and 9.0 Fe-ZIF catalysts; (**c**) The molecule structure of D1 (FeN_4C_8) and D2 (FeN_4C_{10}); (**d**) elemental composition; (**e**) fraction of various types of nitrogen doping for various Fe-ZIF catalysts as function of Fe doping content in ZIF precursors.

Since the coordination by four nitrogen atoms appears to stabilize atomically dispersed Fe sites in catalysts, nitrogen doping may be crucial to ORR activity. N atoms can be doped at either edge or bulk of the graphene planes as the pyridinic and graphitic N with different binding energies of *ca.* 398.6 and 401.1 eV, respectively. We found that N doping is largely dependent on the content of doped Fe. The pyridinic nitrogen peak at 398.3 eV in the Fe-free ZIF sample is shifted positively to 398.7 eV in Fe-ZIF catalysts (**Figure 2b**). This shift is likely attributed to an increase in the oxidation state of nitrogen due to the Fe-N bonds formation. The best performing 1.5Fe-ZIF catalyst has the highest total and pyridinic nitrogen contents of all studied catalysts (**Figures 2d-2e**). This is related to the highest concentration of FeN_4 sites, most likely involving pyridinic nitrogen atoms. The ratio of N to Fe in the 1.5Fe-ZIF catalyst is approximately 7:1, which is higher than the expected stoichiometric ratio of 4:1, indicating that a significant fraction of nitrogen in 1.5Fe-ZIF is not coordinated to Fe at all. Notably, the N content in catalysts tends to decrease with an increase Fe content above 1.5 at.%, implying a loss of N atoms lose from atomic Fe-N_4 sites as a result of Fe clustering at high Fe content.[35]

Catalyst morphology and structures

To understand the effect of Fe doping in the precursor on the structure and morphology of resulting Fe-N-C catalysts, we performed thorough characterization of the precursors and catalysts as a function of the Fe content. The XRD patterns for the Fe-ZIF precursors were found to be independent of the Fe content (Figure S3a), indicating that Fe doping does not affect the ZIF crystallinity. After a single heat treatment at 1100 °C, the XRD patterns were dominated by carbon peaks. The broad peak at 25° implies the presence of dominant amorphous carbon structures in all studied samples (Figure S3b). The 9.0Fe-ZIF catalyst contains small amount of crystalline phases, likely Fe or/and Fe_3C particles.

The effect of the Fe content on the carbon structure was further studied using Raman spectroscopy (**Figure S4**). There is no significant differences between "Fe-free" and 1.5Fe-ZIF catalysts. The similar values of I_D/I_G suggest that they have nearly identical carbon structures. However, an increase in the Fe content to 9.0 at.% results in a rise in D and G bands, which

have similar intensity (the I_D/I_G ratio of 1.0). Although the higher value of I_D/I_G in this case may indicate carbon structure still rich in disorder phase, the narrowness of the D band and the appearance of 2D band at 2700 cm^{-1} suggest overall improvement of the carbon crystallinity.[41] These results point to an enhancement in the degree of graphitization in the 9.0Fe-ZIF catalyst. The subtle changes in the catalyst carbon structures were also studied using HR-TEM images (**Figure S5**). The micrographs are in good agreement with the Raman spectra, indicating an increase in the graphitization of Fe-ZIF catalysts with higher Fe content in precursors, linked to iron-catalyzed formation of graphene shells around the Fe or/and FeC_3 nanoparticles (Figure S5). The surface area and porosity of Fe-doped precursors are nearly independent of the Fe content (**Figures S6** and **S7)**. All ZIF precursors show similar BET surface area of around 1100 m^2/g. However, the high-temperature treatment, *e.g.*, at 1100 °C, leads to significant reduction in the surface area of catalysts to *ca*. 640 m^2/g for 1.5Fe catalyst. This is mainly due to the loss of microporosity, evidenced by a decrease in the N_2 uptake at low pressures.

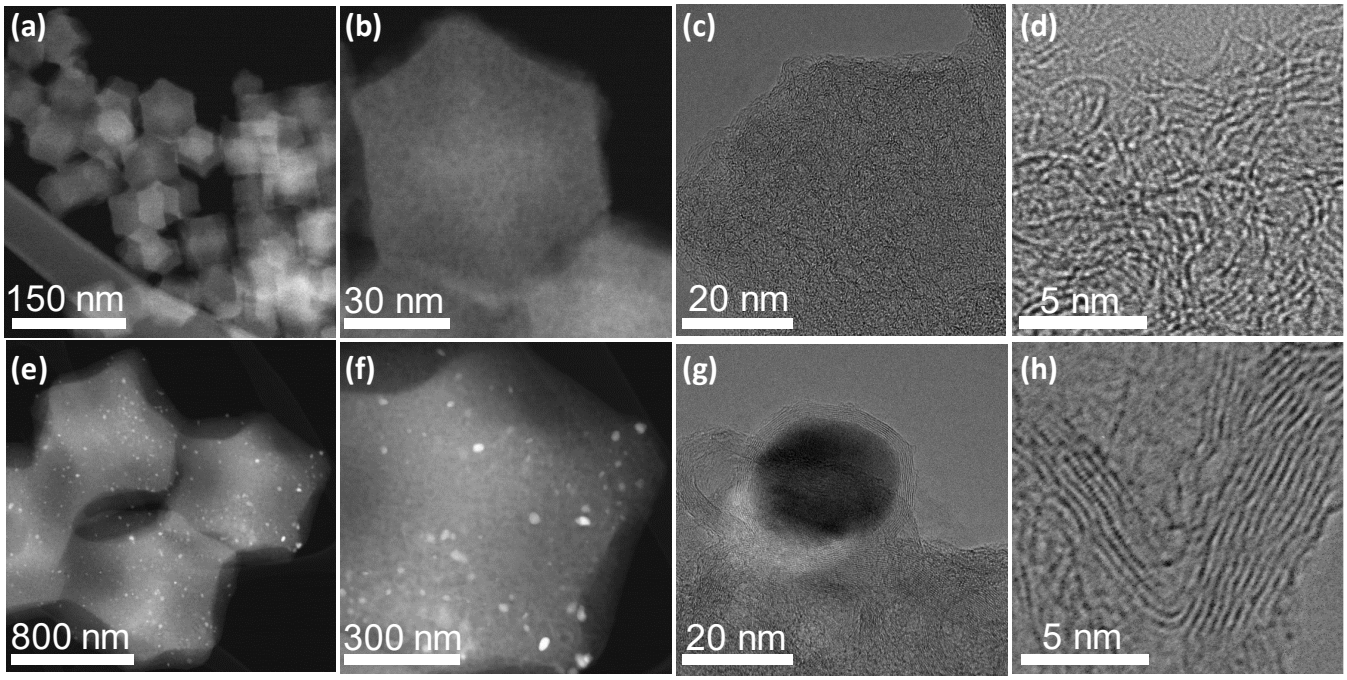

Figure 3. Comparison of catalyst morphology and carbon microstructure in catalysts obtained from Fe-ZIF precursors with (**a-d**) optimum (1.5 at.%) and (**e-h**) high (9.0 at.%) Fe content.

An Fe contents higher than 1.5 at.% results in a decrease in the catalyst surface area due to a less porous graphitic carbon catalyzed by metallic Fe clusters or nanoparticles.[42]

The effect of Fe content on the size of Fe-doped ZIF precursor nanocrystals was studied by scanning electron microscopy (SEM) (**Figure S8**). Fe doping leads to an increase in the ZIF crystal sizes from 40 nm, an average value for the "Fe-free" ZIF-8, to 60 nm and 800 nm for ZIFs doped with of 1.5 at.% and 9.0 at.% of Fe, respectively. In principle, crystal sizes are decided by the relative rates between seed nucleation and growth. The formation of larger particles can be explained by the nucleation rate of seeds becoming slower with an increase in the Fe content during the ZIF crystal formation, possibly because of the competition of Fe^{3+} ions with Zn^{2+} ions to coordinate 2-methylimidazole.[43] While the morphology of Fe-doped ZIF precursors is retained in catalysts, the "Fe-free" ZIF-8 precursor collapses during the high-temperature treatment, yielding resulting in irregular particles and disordered carbon morphology with low level of graphitization (**Figure S9)**. Consequently, Fe doping appears to be preventing 3D ZIFs from collapsing.

To elucidate the impact of Fe on the catalyst structure, we compared two catalysts derived from precursors with the optimum (1.5 at.%) and high (9.0 at.%) Fe content. As shown in **Figures 3** and **S10**, the catalyst derived from ZIF precursors with 1.5 at.% Fe maintains the polyhedron morphology, free of any metallic aggregates. The carbon phase in the 1.5Fe-ZIF catalyst is uniform, dominated by curved carbon fringes, characteristic of the dominant amorphous carbon. In turn, the dominant morphological feature in the 9.0Fe-ZIF catalyst is much larger carbon particles. The carbon polyhedrons are on a *ca*. 1000 nm scale and tend to fuse together, a shape contrast with smaller, isolated polyhedron particles in the 1.5Fe-ZIF catalyst. The catalyst derived from 9.0 at.% Fe precursor also contains numerous metallic aggregates, protected by several layers of highly graphitized carbon shells (**Figure S5**). This feature is often observed with the early Fe-N-C catalysts.[42, 44, 45] In general, highly graphitized Fe-based catalysts are less ORR active in acidic environments, possibly due to the very low content of defects needed for hosting the FeN_4 sites.[17]

Catalyst performance

The ORR activity of catalysts derived from Fe-doped ZIF precursors with Fe content ranging from 0.1 to 9.0 at.% was evaluated using the rotating ring disk electrode (RRDE) in O_2-sa-

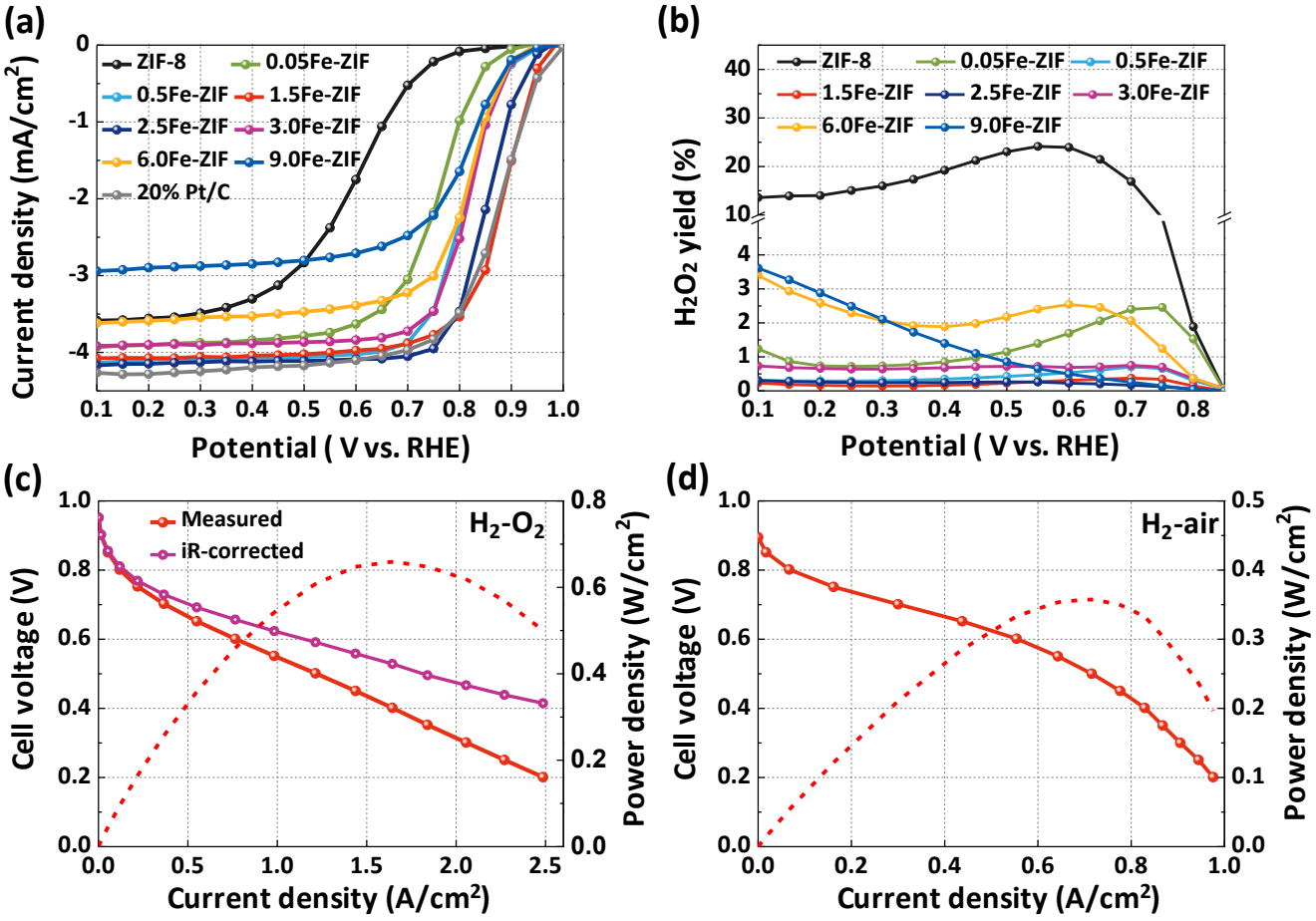

Figure 4. (a) RRDE ORR polarization plots and (b) H_2O_2 yield plots for different Fe-ZIF catalysts as a function of Fe content in the precursor (from 0 to 9 at.%). Test conditions: O_2-saturated 0.5 M H_2SO_4, disk rotation rate 900 rpm, catalyst loading 0.8 mg/cm^2. Fuel cell performance of the 1.5Fe-ZIF catalyst: (c) H_2-O_2 and (d) H_2-air. Anode: 0.2 mg$_{Pt}$/cm^2 Pt/C; H_2 flow rate 200 sccm, 1.0 bar H_2 partial pressure; cathode: *ca.* 4.0 mg/cm^2, 200 sccm gas flow rate, 1.0 bar total partial pressures of gases flown; membrane: Nafion®211; cell: 80°C, 100% RH, 5.0 cm^2 MEA electrode area.

-turated 0.5 M H_2SO_4 electrolyte at 900 rpm and 25°C (**Figures 4a** and **S11-S12**). The loading of all PGM-free catalysts on the disk electrode was 0.8 mg/cm^2. A typical Pt/C catalyst (TKK, 20wt% Pt on Vulcan support) with a loading of 0.3 mg/cm^2 (60 μg$_{Pt}$/cm^2) was studied in 0.1 M $HClO_4$ solution, instead of 0.5 M H_2SO_4 to avoid bisulfate adsorption. The activity increased continuously with an increase in Fe content in precursors from 0 to 1.5 at.%. The performance of the "Fe-free" sample was found to be very poor, as indicated by E_{onset} of 0.82 V and $E_{½}$ of 0.60 V. An addition of even small amount of Fe (0.05 at.%) to the precursor resulted in a significant increase in the ORR activity, with E_{onset} and $E_{½}$ rising to 0.92 V and 0.77 V, respectively. Such a dramatic increase in ORR activity highlights the key role of Fe and the intrinsic activity of FeN_4 sites.[46, 47] A gradual increase in the Fe content in the precursor to 1.5 at.% Fe gives rise to the $E_{½}$ of 0.88 ± 0.01 V. Given the high sensitivity of the $E_{½}$ values to any in homogeneity and variations in the thickness of catalyst layers on disk electrodes, the RDE experiments were repeated several times. The error bars for the polarization data are shown in **Figure S11e-f**. The dramatically enhanced ORR activity with an increase in the Fe content in the precursor up to 1.5 at.% is due to an increase in the density of FeN_4 active sites in the 3D carbon derived from ZIF-8 after the heat treatment. This RDE performance was compared in this work to other similar published research (**Table S1**). The $E_{½}$ of 0.88 ± 0.01 V represents the ever recorded activity for Fe-N-C catalysts. At a high catalyst loading used, the measured $E_{½}$ approaches those for Pt/C catalysts at a disk loading of 60 μg$_{Pt}$/cm^2 (*i.e.*, total 0.3 mg/cm^2 including both carbon and Pt).[48] However, further increase in Fe content in precursors up to 2.5 and 3.0 at.% resulted in obvious drops in the $E_{½}$ value to 0.85 and 0.82 V, respectively, suggesting reduction in the density of active sites due to the formation of Fe clusters or/and FeC_3. This downward trend in the activity continued up to the highest studied Fe content of 9.0 at.%. Since the change in Fe content in the precursor from 1.5 to 2.5 at.% was found to

significantly affect ORR activity of the resulting Fe-N-C catalysts, further optimization of the Fe content was performed in a narrow range between 1.2 to 2.5 at.% (**Figure S11d**). The highest ORR activity was measured with catalysts derived from precursors containing between 1.5-1.8 at.% Fe. This contents correspond to the top of a volcano curve describing the dependence of ORR activity on the Fe content in the ZIF-8 precursors. The continuous increase in ORR activity with an increase in Fe content of ZIF-8 precursors from 0 to 1.5 at.% attests to the dependence of ORR activity on the number of FeN_4 sties. Once the Fe content in precursors reaches a certain threshold, clustering of single atomic Fe sites occurs during the heating treatment, which significantly reduces the number of FeN_4 active sites. This observation can serve as a guidance for designing advanced Fe-N-C catalysts targeting an increase higher content of atomically dispersed Fe for ORR activity enhancement. The density of FeN_4 active sites in the best performing 1.5Fe-ZIF catalyst was also approximately estimated using a method developed by Sahraie *et al*.[6] The maximum mass-based site density (MSD_{max}) and TOF values are found to be 1.3×10^{20} (site/g_{cat}) and 2.1 (e s^{-1}site^{-1}), respectively. They are one of the highest values of MSD_{max} and TOF reported to date for PGM-free catalysts (Table S2),

The electrochemically accessible surface area (ECSA) was estimated from the double layer capacitance as determined using cyclic voltammetry (CV) in N_2 saturated 0.5 M H_2SO_4 electrolyte.[49] It should be noted that the ECSA of catalysts are often lower than the corresponding BET surface areas measured by N_2 isothermal absorption/desorption. The possible reason for the observed difference between ECSA and BET surface areas is the presence of ultra-small micropores in catalyst, which are accessible to N_2 molecules in the gas adsorption studies, but not to H_2O in an aqueous electrolyte. Both the ECSAs and BET surface area value difference with an increase in Fe content **(Figure S12** and **Table S3**). This reduced surface area of catalysts combined with the loss of FeN_4 sites due to clustering likely further accelerate activity decline of catalysts with high Fe content.

The values of H_2O_2 yield as a function of Fe content in the precursor were determined in RRDE experiments (**Figure 4b**). The highest H_2O_2 yield was measured with the catalyst synthesized from a Fe-free ZIF precursor (15-20%). Peroxide yields were significantly lower for catalysts synthesized using Fe-doped ZIF precursors, reaching values below 1% for the 1.5Fe-ZIF catalyst at a loading of 0.8 mg cm^{-2} (error bars provided in Figure S11). This result points to significant contribution of the four-electron path in the ORR and/or to an increase in the rate of the 2e+2e process. However, the catalysts with higher Fe content, the 9.0Fe-ZIF catalyst in particular, generated relatively high H_2O_2 yields of 3-4% during the ORR.

The best performing 1.5Fe-ZIF catalyst was used for fabricating membrane electrode assemblies (MEAs) studied in fuel cells on both O_2 and air. The purpose of studying fuel cell performance on O_2 (1.0 bar partial pressure) was to minimize mass-transport losses when determining catalyst activity in MEAs (**Figure 4c**). An open cell voltage (OCV) measured with an MEA was 0.98 V, in good agreement with RDE tests in acidic electrolytes, only *ca*. 20 mV lower than the value measured with a Pt/C cathode (0.2 mg_{Pt}/cm^2) under the same conditions.[44] The current density generated at a reference fuel cell voltage of 0.80 V was 145 mA/cm^2, which is more than double the current density measured previously with a Fe-N-C catalyst derived from polyaniline in 2011 (ca. 70 mA/cm^2, at a much higher O_2 partial pressure of 2.3 bar).[44] This result shows that the high ORR activity measured in aqueous electrolytes can be realized in polymer electrolyte in the fuel cell cathode. An MEA with the 1.5Fe-ZIF catalyst in the cathode was also studied under air at a total partial pressure of 1.0 bar (O_2 partial pressure of *ca.* 0.2 bar). The OCV value decreased by only 30 mV relative to that measured on O_2, from 0.98 to 0.95 V, and the current density at 0.80 V dropped by nearly 50%, from 145 to 75 mA/cm^2 (**Figure 4d**), typical for oxygen- and air-operated cathodes. The H_2-air performance in this work is still one of the highest reported to date for PGM-free catalysts (**Table S4**)[1, 44].

Stability of Fe-N-C cathode catalysts in acidic media represents a major challenge especially at high potentials (> 0.6 V). According to U.S. DOE, dynamic voltage cycling between 0.6 and 1.0 V or voltage hold at constantly are more relevant to real fuel cell operation. In this work, we employed two stability testing protocols, including potential cycling and holding constant potential/voltage to evaluate durability of the atomically dispersed Fe-N-C catalysts. A 40,000 accelerated stress test (AST) potential cycles (0.6-1.0 V) in O_2 saturated 0.5 M H_2SO_4 electrolyte led to only 30 mV loss in the $E_{½}$ value (**Figure 5a**), attesting much improved catalyst stability, compared to that of an earlier Fe-N-C catalyst, which lost 80 mV after only 5000 cycles.[50] The post-mortem microscopy analysis indicates that atomically dispersed and nitrogen-coordinated Fe sites are still clearly visible in the 1.5Fe-ZIF catalyst after the AST test (**Figures 5b-c** and **S13**), attesting to very good stability of a majority of FeN_4 sites during the dynamic potential cycling test. The morphology of carbon particles remainsed intact, with nearly identical sizes and clear edges of polyhedral particles, as the catalysts before the AST (**Figure S14**), suggesting insignificant carbon corrosion.

We also conducted constant-potential testing of the catalyst by holding potential at a relatively high potential of 0.85 V in O_2 saturated 0.5 M H_2SO_4 for 100 hours (**Figure 5d**). We recorded ORR polarization plots every 10 hours, finding ORR activity partially recover every time a polarization plot was recorded in the range from 0 to 1.0 V. However, the rate of unrecoverable degradation remained unchanged throughout the test. In the end, the catalyst suffered from significant decrease in the ORR activity, especially in the first 20 hours, when approximately half of the initial ORR activity was lost. At the end of the 100-hour test, the remaining activity was only 30% of that measured initially. The HAADF-STEM images indicate a severe carbon corrosion, with catalyst particles becoming rounded and agglomerated (**Figure S15**).

Journal Name

ARTICLE

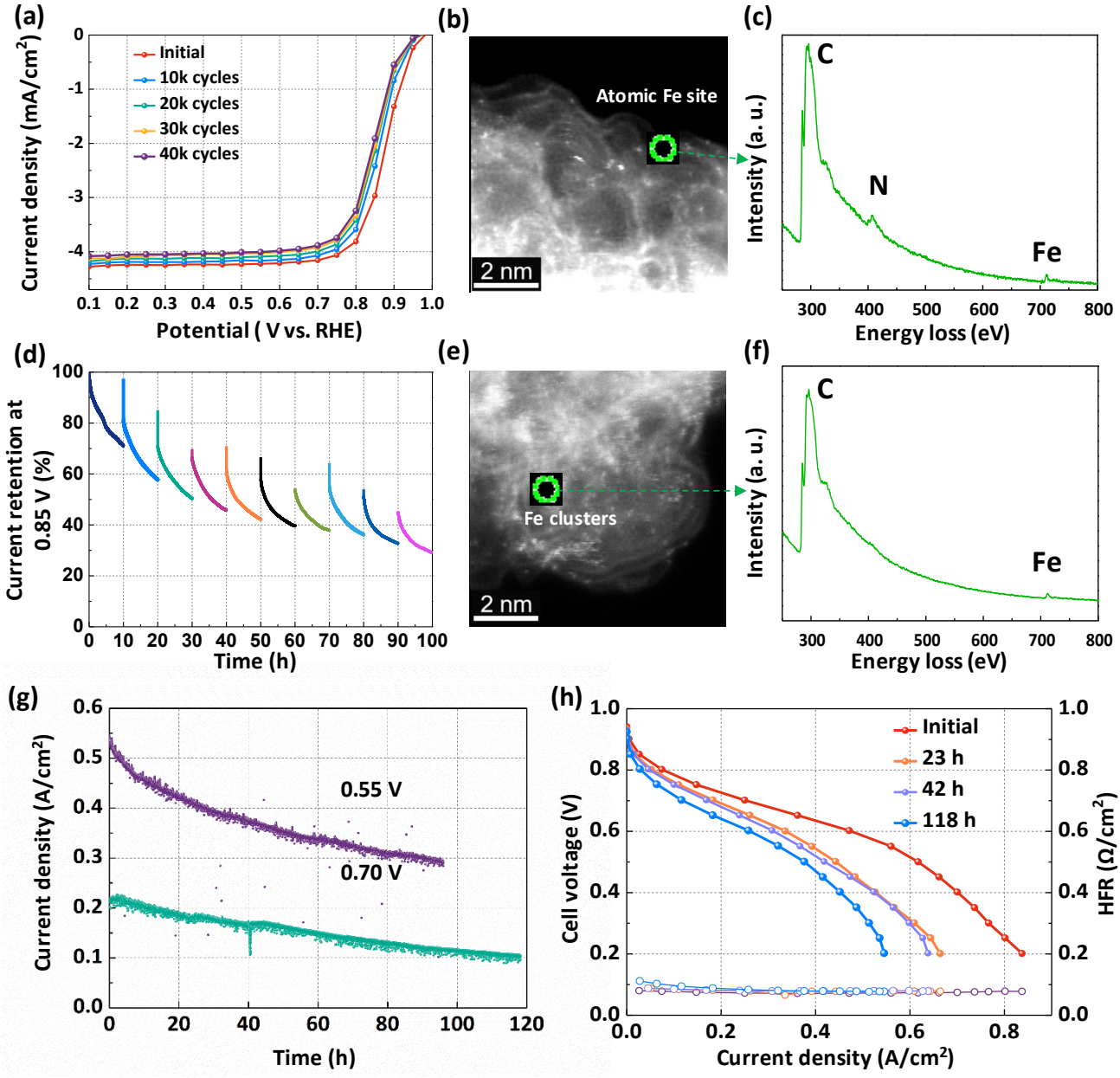

Figure 5. (**a, d**) RDE stability tests of the best performing 1.5Fe-ZIF catalyst in O_2-saturated 0.5 M H_2SO_4 electrolyte using different test protocols. Structural changes by (b-c) STEM and (e-f) EELS analysis. (**a-c**) Potential cycling between 0.60 and 1.0 V still showing significant atomically dispersed Fe sites coordinated by N. (**d-f**) Holding at a constant potential of 0.85 V for 100 hours, significant degradation especially at the initial stage accompanying with depicting appearance of Fe clusters and likely Fe-N bond breaking or weakening. (**g**) Fuel cell durability tests at a constant potential of 0.70 V and 0.55 V, respectively. (**h**) Fuel cell polarization plots recorded at different times during the 120-hour durability test at 0.70 V. Fuel cell cathode: catalyst loading 4.0 mg/cm^2; 100% RH; air flown at 200 sccm, 1.0 bar total partial pressure of gases. Anode: Pt/C, 0.20 mg_{Pt}/cm^2, 100% RH; H_2 flown at 200 sccm, 1.0 bar partial gas pressure. Membrane: Nafion® 212. Temperature: 80 °C. MEA area: 5.0 cm^2.

Journal Name

ARTICLE

While a majority of atomically dispersed sites are still present after the durability test, some iron clusters become apparent. The Fe atoms in those clusters appear no longer coordinated by nitrogen (**Figures 5e-f**), since Fe and N EELS signals cannot be detected simultaneously at the atomic level. The possible degradation mechanisms involve the cleavage of Fe-N coordination likely due Fe oxidation and carbon corrosion in the catalyst. Carbon corrosion may be also responsible for the loss of Fe-N coordination due to weakening of the Fe-N and N-C bonds ultimately resulting in decomposition of FeN_4 sites.[51, 52] If independently confirmed, these degradation mechanisms set a possible path towards stabilizing Fe-N-C catalysts *via* making carbon structure more robust and corrosion-resistant, especially next to the active site(s).

Finally, the life tests of MEAs were performed in H_2-air fuel cells at constant voltages of 0.55 V and 0.70 V for approximately 100 hours **(Figure 5g**). While performance degrades at both voltages, the tests reveal, perhaps for the first time, that atomically dispersed Fe catalysts can sustain respectable current densities at practically relevant voltages for prolonged times. Fuel cell polarization plots recorded at different times during the life test at 0.70 V are shown in **Figure 5h**. They indicate similar performance losses across the entire range of fuel cell voltages. The current density loss at 0.80 V is *ca.* 30 mA/cm^2 after the first 23 hours, but much less later on (35 mA/cm^2 after 42 hours and 46 mA/cm^2 at the end of the 118-hour test). Similarly, at a low voltage of 0.40 V, the total loss in current density during the test is 35%, with most of it happening in the first 23 hours.

Compared to aqueous acidic electrolytes, performance degradation in fuel cell MEAs is much more complex with several mechanisms possible.[53] In addition to catalyst degradation due to demetalation and carbon corrosion, degradation of three-phase (gas, liquid, solid) interfaces and water flooding in micropores may lead to severe proton and mass transfer resistances. It should be noted that, unlike in aqueous electrolytes, the confined H_2O_2 formation within the fuel cell cathode could be more harmful than an aqueous electrolyte resulting in the free radicals known to cause active site degradation and carbon corrosion.[53] In this study, performance degradation of the Fe-N-C catalyst in MEAs was found to be comparable at 0.55 V and 0.70 V (*ca.* 45-50% current loss). However, the causes of performance loss could be different in these two cases. At a lower voltage of 0.55 V, catalyst degradation may be due to relatively high amount of generated H_2O_2, resulting in a higher than at 0.70 V yields of hydroperoxyl, known to be highly detrimental to both the ionomer and carbon. At a higher voltage of 0.70 V, the performance loss is more likely to be caused by accelerated carbon corrosion and the ensuing deterioration of the carbon matrix hosting FeN_4 sites. Further studies under various operating conditions are necessary to identify the causes of the PGM-free cathode degradation and address the stability challenge before PGM-free catalysts become viable for PEFC applications.

Conclusions

FeN_4 sites have been considered the most likely ORR active sites in PGM-free catalysts in acidic media. In this work, we developed a chemical method for precisely controlling the Fe content in ZIF-8 precursors (from 0 to 9 at.%). Through fine-tuning and optimizing Fe content to 1.5 at.%, we obtained a catalyst with fully atomically dispersed and nitrogen-coordinated FeN_4 sites, free of any metal-rich clusters and nanoparticles. This catalyst with the highest density of active sites yields the best ORR activity. A higher than optimum Fe content in the precursor results in the formation of clusters and nanoparticles that "consume" Fe atoms reducing the number of active sites in the catalyst. The volcano-like dependence between the ORR activity and Fe content provides an insight into the role of Fe in Fe-N-C ORR catalysts. Using these model catalysts with controlled Fe content, we also described the effect of Fe in precursors on catalyst morphologies and structures such as particle size, porosity, nitrogen-doping level, and carbon microstructure. The excess Fe negatively impacts the catalyst performance. In particular, high Fe content leads to larger catalyst particles, reduced surface area, and pore volume. The Fe clusters and nanoparticles also catalyze carbon graphitization, limiting the number of carbon defects as hosts for active sites.

The highly dispersed FeN_4 sites in catalysts appear to be directly responsible for the record-high ORR activity of PGM-free catalysts in RDE testing and in the fuel cell cathode. Stability studies by potential cycling (0.6-1.0 V) and at a constant high potential of 0.85 V, along with *post mortem* microscopy, suggest that the loss of Fe-N coordination and significant carbon corrosion are responsible for the ORR activity decrease in acidic aqueous electrolytes. Although the durability of the catalyst with atomically dispersed FeN_4 sites at a practically relevant voltage 0.7 V is encouraging, the stability challenges need to be overcome before PGM-free catalysts become viable for fuel cell applications.

Conflicts of interest

There are no conflicts to declare.

Acknowledgements

This work was financially supported with start-up funding from the University at Buffalo, SUNY. Materials synthesis and characterization effort was also supported by National Science Foundation (CBET-1604392, 1804326). Financial support from the DOE-EERE Fuel Cell Technologies Office is gratefully acknowledged. We thank Dr. Ye Lin for XPS data analysis. Electron microscopy research was conducted in the Center for Nanophase Materials Sciences of Oak Ridge National Laboratory, which is a DOE Office of Science User Facility. U.I.K. and S.W. would like to acknowledge financial support by German Research Foundation (GSC1070) and the Federal Ministry of Education and Research (05K16RD1).

References

1. H. T. Chung, D. A. Cullen, D. Higgins, B. T. Sneed, E. F. Holby, K. L. More and P. Zelenay, *Science*, 2017, **357**, 479-484.
2. M. Shao, Q. Chang, J.-P. Dodelet and R. Chenitz, *Chem. Rev.*, 2016, **116**, 3594-3657.
3. A. Zitolo, V. Goellner, V. Armel, M.-T. Sougrati, T. Mineva, L. Stievano, E. Fonda and F. Jaouen, *Nat. Mater.*, 2015, **14**, 937-942.
4. S. Kattel and G. Wang, *The journal of physical chemistry letters*, 2014, **5**, 452-456.
5. E. F. Holby, G. Wu, P. Zelenay and C. D. Taylor, *The Journal of Physical Chemistry C*, 2014, **118**, 14388-14393.
6. N. R. Sahraie, U. I. Kramm, J. Steinberg, Y. Zhang, A. Thomas, T. Reier, J.-P. Paraknowitsch and P. Strasser, *Nature Communications*, 2015, **6**, 8618.
7. G. Wu, A. Santandreu, W. Kellogg, S. Gupta, O. Ogoke, H. Zhang, H.-L. Wang and L. Dai, *Nano Energy*, 2016, **29**, 83-110.
8. Z. Qiao, H. Zhang, S. Karakalos, S. Hwang, J. Xue, M. Chen, D. Su and G. Wu, *Applied Catalysis B: Environmental*, 2017, **219**, 629-639.
9. H. Zhang, H. Osgood, X. Xie, Y. Shao and G. Wu, *Nano Energy*, 2017, **31**, 331-350.
10. J. Liu, D. Zhu, C. Guo, A. Vasileff and S.-Z. Qiao, *Advanced Energy Materials*, 2017, **7**, 1700518.
11. H. M. Barkholtz and D.-J. Liu, *Materials Horizons*, 2017, **4**, 20-37.
12. E. Proietti, F. Jaouen, M. Lefèvre, N. Larouche, J. Tian, J. Herranz and J.-P. Dodelet, *Nat. Commun.*, 2011, **2**, 416.
13. W. Xia, J. Zhu, W. Guo, L. An, D. Xia and R. Zou, *Journal of Materials Chemistry A*, 2014, **2**, 11606-11613.
14. D. Zhao, J. L. Shui, L. R. Grabstanowicz, C. Chen, S. M. Commet, T. Xu, J. Lu and D. J. Liu, *Advanced Materials*, 2014, **26**, 1093-1097.
15. P. Yin, T. Yao, Y. Wu, L. Zheng, Y. Lin, W. Liu, H. Ju, J. Zhu, X. Hong and Z. Deng, *Angewandte Chemie International Edition*, 2016, **55**, 10800-10805.
16. H. Zhang, J. Nai, L. Yu and X. W. D. Lou, *Joule*, 2017, **1**, 77-107.
17. X. Wang, H. Zhang, H. Lin, S. Gupta, C. Wang, Z. Tao, H. Fu, T. Wang, J. Zheng, G. Wu and X. Li, *Nano Energy*, 2016, **25**, 110-119.
18. J. Li, M. Chen, D. A. Cullen, S. Hwang, M. Wang, B. Li, K. Liu, S. Karakalos, M. Lucero, H. Zhang, C. Lei, H. Xu, G. E. Sterbinsky, Z. Feng, D. Su, K. L. More, G. Wang, Z. Wang and G. Wu, *Nature Catalysis*, 2018, **1**, 935-945.
19. Y. He, S. Hwang, D. A. Cullen, M. A. Uddin, L. Langhorst, B. Li, S. Karakalos, A. J. Kropf, E. C. Wegener, J. Sokolowski, M. Chen, D. Myers, D. Su, K. L. More, G. Wang, S. Litster and G. Wu, *Energy & Environmental Science*, 2019, **12**, 250-260.
20. X. X. Wang, D. A. Cullen, Y.-T. Pan, S. Hwang, M. Wang, Z. Feng, J. Wang, M. H. Engelhard, H. Zhang, Y. He, Y. Shao, D. Su, K. L. More, J. S. Spendelow and G. Wu, *Advanced Materials*, 2018, **30**, 1706758.
21. P. Su, H. Xiao, J. Zhao, Y. Yao, Z. Shao, C. Li and Q. Yang, *Chemical Science*, 2013, **4**, 2941-2946.
22. T. Liu, P. Zhao, X. Hua, W. Luo, S. Chen and G. Cheng, *Journal of Materials Chemistry A*, 2016, **4**, 11357-11364.
23. S. Zhao, H. Yin, L. Du, L. He, K. Zhao, L. Chang, G. Yin, H. Zhao, S. Liu and Z. Tang, *ACS nano*, 2014, **8**, 12660-12668.
24. L. Zhang, K. Lee, C. W. B. Bezerra, J. Zhang and J. Zhang, *Electrochimica Acta*, 2009, **54**, 6631-6636.
25. F. Jaouen, S. Marcotte, J.-P. Dodelet and G. Lindbergh, *The Journal of Physical Chemistry B*, 2003, **107**, 1376-1386.
26. M. Lefèvre, J. P. Dodelet and P. Bertrand, *The Journal of Physical Chemistry B*, 2002, **106**, 8705-8713.
27. S. Li, L. Zhang, H. Liu, M. Pan, L. Zan and J. Zhang, *Electrochimica Acta*, 2010, **55**, 4403-4411.
28. B. You, N. Jiang, M. Sheng, W. S. Drisdell, J. Yano and Y. Sun, *ACS Catalysis*, 2015, **5**, 7068-7076.
29. V. Ordomsky, B. Legras, K. Cheng, S. Paul and A. Khodakov, *Catalysis Science & Technology*, 2015, **5**, 1433-1437.
30. L. Shang, H. Yu, X. Huang, T. Bian, R. Shi, Y. Zhao, G. I. N. Waterhouse, L.-Z. Wu, C.-H. Tung and T. Zhang, *Advanced Materials*, 2016, **28**, 1668-1674.
31. V. Armel, S. Hindocha, F. Salles, S. Bennett, D. Jones and F. Jaouen, *Journal of the American Chemical Society*, 2017, **139**, 453-464.
32. H. Zhang, S. Hwang, M. Wang, Z. Feng, S. Karakalos, L. Luo, Z. Qiao, X. Xie, C. Wang, D. Su, Y. Shao and G. Wu, *Journal of the American Chemical Society*, 2017, **139**, 14143-14149.
33. G. Wu and P. Zelenay, *Accounts of chemical research*, 2013, **46**, 1878-1889.
34. X. J. Wang, J. W. Zhou, H. Fu, W. Li, X. X. Fan, G. B. Xin, J. Zheng and X. G. Li, *Journal of Materials Chemistry A*, 2014, **2**, 14064-14070.
35. U. I. Kramm, I. Herrmann-Geppert, S. Fiechter, G. Zehl, I. Zizak, I. Dorbandt, D. Schmeißer and P. Bogdanoff, *J. Mater. Chem. A*, 2014, **2**, 2663–2670.
36. K. Liu, G. Wu and G. Wang, *The Journal of Physical Chemistry C*, 2017, **121**, 11319-11324.
37. U. I. Kramm, L. Ni and S. Wagner, *Advanced Materials*, 2019, **31**, 201805623.
38. U. I. Koslowski, I. Abs-Wurmbach, S. Fiechter and P. Bogdanoff, *The Journal of Physical Chemistry C*, 2008, **112**, 15356-15366.
39. U. I. Kramm, J. Herranz, N. Larouche, T. M. Arruda, M. Lefèvre, F. Jaouen, P. Bogdanoff, S. Fiechter, I. Abs-Wurmbach and S. Mukerjee, *Physical Chemistry Chemical Physics*, 2012, **14**, 11673-11688.
40. U. I. Kramm, I. Abs-Wurmbach, I. Herrmann-Geppert, J. Radnik, S. Fiechter and P. Bogdanoff, *J. Electrochem. Soc.*, 2011, **158**, B69-B78.
41. M. Pawlyta, J.-N. Rouzaud and S. Duber, *Carbon*, 2015, **84**, 479-490.

42. V. Nallathambi, J.-W. Lee, S. P. Kumaraguru, G. Wu and B. N. Popov, *Journal of Power Sources*, 2008, **183**, 34-42.
43. J. K. Zaręba, M. Nyk and M. Samoć, *Crystal Growth & Design*, 2016, **16**, 6419-6425.
44. G. Wu, K. L. More, C. M. Johnston and P. Zelenay, *Science*, 2011, **332**, 443-447.
45. H. T. Chung, J. H. Won and P. Zelenay, *Nature Communications*, 2013, **4**, 1922.
46. E. F. Holby, G. Wu, P. Zelenay and C. D. Taylor, *J. Phys. Chem. C*, 2014, **118**, 14388–14393.
47. S. Kattel and G. Wang, *Journal of Materials Chemistry A*, 2013, **1**, 10790-10797.
48. C. Chen, Y. Kang, Z. Huo, Z. Zhu, W. Huang, H. L. Xin, J. D. Snyder, D. Li, J. A. Herron, M. Mavrikakis, M. Chi, K. L. More, Y. Li, N. M. Markovic, G. A. Somorjai, P. Yang and V. R. Stamenkovic, *Science*, 2014, **343**, 1339-1343.
49. X. Wang, Q. Li, H. Pan, Y. Lin, Y. Ke, H. Sheng, M. T. Swihart and G. Wu, *Nanoscale*, 2015, **7**, 20290-20298.
50. G. Wu, M. A. Nelson, N. H. Mack, S. Ma, P. Sekhar, F. H. Garzon and P. Zelenay, *Chemical Communications*, 2010, **46**, 7489-7491.
51. U. I. Kramm, M. Lefèvre, P. Bogdanoff, D. Schmeißer and J.-P. Dodelet, *The Journal of Physical Chemistry Letters*, 2014, DOI: 10.1021/jz501955g, 3750–3756.
52. V. Goellner, C. Baldizzone, A. Schuppert, M. T. Sougrati, K. Mayrhofer and F. Jaouen, *Phys. Chem. Chem. Phys.*, 2014, **16**, 18454–18462.
53. X. X. Wang, V. Prabhakaran, Y. He, Y. Shao and G. Wu, *Advanced Materials*, 2019, **31**, 1805126.

Graphitic Abstract: